ACS OMEGA

http://pubs.acs.org/journal/acsodf

Article

Synthesis and Characterization of Silver-Coated Polymeric Scaffolds for Bone Tissue Engineering: Antibacterial and In Vitro Evaluation of Cytotoxicity and Biocompatibility

Muhammad Umar Aslam Khan, Saiful Izwan Abd Razak,* Hassan Mehboob, Mohammed Rafiq Abdul Kadir, T. Joseph Sahaya Anand, Fawad Inam, Saqlain A. Shah, Mahmoud E. F. Abdel-Haliem, and Rashid Amin*

Cite This: *ACS Omega* 2021, 6, 4335−4346

Read Online

ACCESS | Metrics & More | Article Recommendations

ABSTRACT: In bone tissue engineering, multifunctional composite materials are very challenging. Bone tissue engineering is an innovative technique to develop biocompatible scaffolds with suitable orthopedic applications with enhanced antibacterial and mechanical properties. This research introduces a polymeric nanocomposite scaffold based on arabinoxylan-*co*-acrylic acid, nano-hydroxyapatite (nHAp), nano-aluminum oxide (nAl_2O_3), and graphene oxide (GO) by free-radical polymerization for the development of porous scaffolds using the freeze-drying technique. These polymeric nanocomposite scaffolds were coated with silver (Ag) nanoparticles to improve antibacterial activities. Together, nHAp, nAl_2O_3, and GO enhance the multifunctional properties of materials, which regulate their physicochemical and biomechanical properties. Results revealed that the Ag-coated polymeric nanocomposite scaffolds had excellent antibacterial properties and better microstructural properties. Regulated morphological properties and maximal antibacterial inhibition zones were found in the porous scaffolds with the increasing amount of GO. Moreover, the nanosystem and the polymeric matrix have improved the compressive strength (18.89 MPa) and Young's modulus (198.61 MPa) of scaffolds upon increasing the amount of GO. The biological activities of the scaffolds were investigated against the mouse preosteoblast cell lines (MC3T3-E1) and increasing the quantities of GO helps cell adherence and proliferation. Therefore, our findings showed that these silver-coated polymeric nanocomposite scaffolds have the potential for engineering bone tissue.

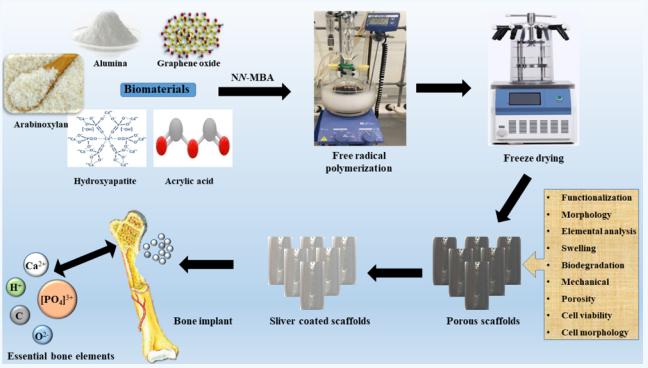

1. INTRODUCTION

Bone tissue engineering is an advanced approach to developing functional scaffolding materials by repairing and regenerating the fractured bone. These functional scaffold materials should be biodegradable and biocompatible that encourage cell adherence, proliferation, and migration to develop new tissue by providing mechanical support and a temporary extracellular matrix.[1] Thus, it is highly desirable to synthesize scaffolds, which are biologically active with sufficient mechanical properties for load-bearing applications.[1,2] Because of their strong bioactivities, natural biodegradable polymers, including chitosan, guar gum, silk fibrin, and so forth, were approved by the United States Food and Drug Administration (USFDA).[3] These polymers possess strong biocompatibility with adoptable biodegradability and processability but inadequate mechanical properties for scaffold applications. Another significant issue is the absence of antibacterial activity to prevent implant-related infections, taking into account the side effects of antibiotics and the severe antibiotic resistance for different bacteria.[4,5] The development of potential materials is challenging to address the problems mentioned above .[6]

Graphene oxide (GO) is a graphene derivative, and it contains oxygen-based functional groups such as hydroxyl, carboxylic, carbonyl, etc. These functional groups are very stable and aligned along edges and over the GO sheet. Because of its exceptional physical, chemical, biological, and extraordinary mechanical characteristics, GO attracts enormous research interests from the researchers.[7] The excellent mechanical properties of GO have turned it into an attractive

Received: November 17, 2020
Accepted: January 14, 2021
Published: February 2, 2021

strengthening filler for polymer composites.[8] Moreover, the oxygen-based functional groups of GO form hydrogen bonding with the oxygenated functional groups of polymers to develop a desirable interfacial adhesion.[9]

Silver nanoparticles have recently attracted considerable interest for antibacterial applications because of their ideal antibacterial behavior. Silver ions play a critical role in antibacterial action because several scientists claimed that Ag^+ has the most potent antibacterial activity among all metal ions.[9,10] Silver nanoparticles may regulate reactive oxygen species (ROS) generation in bacteria, resulting in oxidative damage to cellular components.[11,12]

Hydroxyapatite (HAp) is a well-known bone mineral for bone tissue engineering because of its excellent biocompatibility and physicochemical and biomechanical properties. However, the brittle nature of HAp restricts its application in flexible regimes. Aluminum oxide (Al_2O_3) is an oxidized form of aluminum (Al) and it is a durable, lightweight, and very stable metal. Because of its lightweight, durable nanotopography and available additional active sites, Al_2O_3 supports cell adherence.[13,14] Thus, HAp has been incorporated into polymers to achieve the composite material's desired biomechanical properties.[15,16] Therefore, the selection of biodegradable materials is essential to the synthesis of a polymeric composite and to fabricate composite scaffolds for bone tissue engineering. These composites' physicochemical and biomechanical properties can be tailored, such as swelling, biodegradation, water retention, and wetting.[10,17] Arabinoxylan is a natural polymer and a well-known polysaccharide and found abundantly in woody plants and softwoods. Arabinoxylans make a functioning part of the polymeric matrix within the plant cell wall, and its chemical composition depends on the source. It contains α-L-arabinofuranosyl, α-D-glucopyranosyl uronic acid, and acetyl groups. Cereal cell wall (e.g., barley, husk, oat, and rye) is a rich and active source of arabinoxylans.[18−20] Various groups have used synthetic polymers such as polylactic acid, poly(glycolic acid), and polyvinyl alcohol, and so forth. We have still reported the grafting of ARX with acrylic acid (AAc) as there is relative research available on ARX-*co*-AAc.[21,22]

The GO/nHAp polymer nanocomposite has enhanced mechanical and antibacterial properties because of the targeted interconnected structures. Increasing the GO amount also increases the porosity and interparticle space of composite scaffolds. Probably, the dynamic relationship between GO and Ag enhances not only mechanical properties but also antibacterial activity. GO has unique features like several oxygen-based functional groups, π-conjugation, and a higher surface area.[23] These multifunctional nanocomposites interact with bacterial cellular membranes to hinder bacterial growth because polymeric nanocomposites containing Ag^+/GO have more affinity to contact and kill bacteria.[24]

We have synthesized a novel polymeric nanocomposite (ARX-GO-nHAp/nAl_2O_3-AAc) through free radical polymerization. The porous scaffolds were fabricated from the polymeric nanocomposite (ARX-GO-*g*-nHAp/n-Al_2O_3-AAc) via freeze-drying. To the best of our knowledge, this formulation has never been reported with the same method, which is the novelty of this work. The synthesized polymeric nanocomposite was studied using Fourier transform infrared spectroscopy (FTIR), its surface morphology was determined using scanning electron microscopy (SEM), and the mechanical behavior of scaffolds was studied using the ultimate tensile machine. The swelling analysis was conducted in aqueous and phosphate buffer saline (PBS) solution. The antibacterial activities were conducted against *Escherichia coli*, *Staphylococcus Aureus*, and *Pseudomonas aeruginosa* and cytotoxicity and cell morphology were evaluated using mouse preosteoblast (*MC3T3-E1*) cell lines.

2. EXPERIMENTAL SECTION

2.1. Materials and Methods. *2.1.1. Chemicals.* The husk of *Plantago Ovata* (*P. Ovata*) was purchased from a local market in Johor Bahru (JB), Malaysia. AAc and *N*,*N*′-methylene-bis-acrylamide (*N*,*N*-MBA), nanohydroxyapatite (nHAp, <100 nm particle size), nanoaluminum oxide (nAl_2O_3), GO (CAS# 763713-1G), acetic acid, silver nitrate ($AgNO_3$), PBS solution, sodium hydroxide (NaOH), liquid ammonia, and hydrochloric acid (HCl) were obtained from Sigma-Aldrich, Selangor, Malaysia. These chemicals were used as received.

2.1.2. Biological Materials and Reagents. Mouse preosteoblast (*MC3T3-E1*) cell-lines were obtained from the American Type Culture Collection (ATCC), Manassa, VA, USA, and handled as per ATCC precautions. The α-MEM medium [with ribonucleosides and L-glutamine (Cat# A1049001)], fetal bovine serum (FBS # 10270106), and Pen/Strep (Cat# 15140122) were purchased from Gibco. These chemicals were of analytical grade and used as received.

2.1.3. Extraction of Arabinoxylan. Arabinoxylan was extracted from *P. ovata* husk, as reported by Saghir et al.[25] Briefly, 100 g husk of *P. ovata* was soaked into deionized water overnight, and pH of the solution was adjusted to 12 by adding $NaOH_{(aq)}$. Husk was removed from the gel through vacuum filtration then acetic acid was added to adjust the pH of the coagulated sample to 3. The gel was washed with deionized water to neutralize the pH of the media. Then, the gel was freeze-dried to obtain a dried powder of arabinoxylan.

2.1.4. Synthesis of a Polymeric Nanocomposite Material. The polymeric nanocomposite materials were synthesized via the free radical polymerization method. Arabinoxylan (2 g) was dispersed into deionized water (20 mL) and shifted to a two-neck round bottom flask. nHAp (1.8 g) and n-Al_2O_3 (0.2 g) were dispersed into 10 mL of deionized water and added to the round bottom flask and stirred for 45 min. After 45 min, different amounts of GO (0.2, 0.4, and 0.6 mg) were added into the round bottom flask to obtain the homogeneous solution. Then, the solution was heated at 65 °C in an inert nitrogen atmosphere under constant stirring. AAc (0.50 mL) as a monomer was added after 30 min and *N*,*N*-MBA crosslinker (0.05% of AAc) was added into a round bottom flask. The cross-linking was initiated by adding potassium persulfate (0.05 g) as the initiator and reaction media were heated at 65 °C for 3 h with continuous stirring. nHAp, n-Al_2O_3, and GO were engulfed into the grafted matrix of AAc in ARX. After 3 h, the reaction media were cooled down, nitrogen flow was removed, and reaction media were vacuum filtered. The residue was washed 3−4 times with excessive deionized water to remove unreacted chemicals. These were dried in an oven at 50 °C for 24 h to obtain a dried polymeric nanocomposite material. The proposed chemical reaction has been presented as follows.

The proposed chemical reaction shows the chemical reaction of polymeric materials (arabinoxylan, AAc, and *N*,*N*-MBA) and ceramic materials (nHAp and nanoaluminum

https://dx.doi.org/10.1021/acsomega.0c05596
ACS Omega 2021, 6, 4335−4346

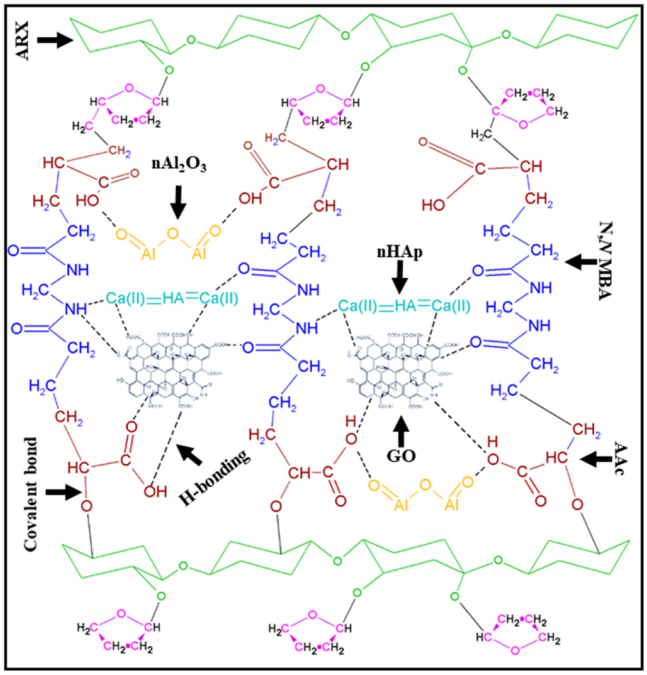

dioxide) and reinforcement (GO) through free-radical polymerization.

2.1.5. Fabrication of Polymeric Nanocomposite Scaffolds. The polymeric nanocomposite scaffolds were fabricated by dispersing the fine powder polymeric nanocomposite (1.2 g) into 10 mL of deionized water and sonicated to prepare a homogeneous slurry. The slurry was filled into a 24-well cell culture plate and kept at −80 °C for 48 h. Then, the samples were freeze-dried to get the porous polymeric nanocomposite scaffolds, as shown in Figure 1.

2.1.6. Coating of a Silver Solution on the Polymeric Nanocomposite Scaffolds. These scaffolds were coated with silver nanoparticles, as reported in our previous studies.[10] Briefly, the fabricated polymeric nanocomposite scaffolds were washed with deionized water to remove the particles. Then, these were treated with 10 wt % $NaOH_{(aq)}$ for 5 min. The silver nitrate ($AgNO_3$) solution (0.45 M) was prepared and liquid ammonia (25 wt %) was added dropwise into the silver nitrate solution. The solution was stirred at 450 rpm to get a clear and a transparent solution of $[Ag(NH_3)_2]^+$ was prepared. The polymeric nanocomposite scaffolds were immersed into the $[Ag(NH_3)_2]^+$ solution for 30 s and then oven-dried at 100 °C for 5 min, as shown in Figure 1. This process was repeated 50 times to deposit a substantial amount of silver nanoparticles onto/into porous polymeric nanocomposite scaffolds. These silver-coated scaffolds were washed with deionized water. These scaffolds were packed in a zip-lock bag to conduct physicochemical and biological characterization. These silver-coated polymeric nanocomposite scaffolds were abbreviated AA-Ag-1, AA-Ag-2, and AA-Ag-3 after adding different amounts of GO (0.2, 0.4, and 0.6 mg), respectively.

2.2. Characterization. *2.2.1. FTIR.* Functional group identification was carried out by FTIR spectroscopy (Nicolet 5700, Waltham, MA, USA). The wavelength range is from 4000 to 400 cm^{-1}, with an average of 150 scans. The morphology and elemental analyses of the scaffolds were carried out by scanning electron microscopy (JSM-6701S) coupled with energy-dispersive X-ray spectroscopy (EDX).

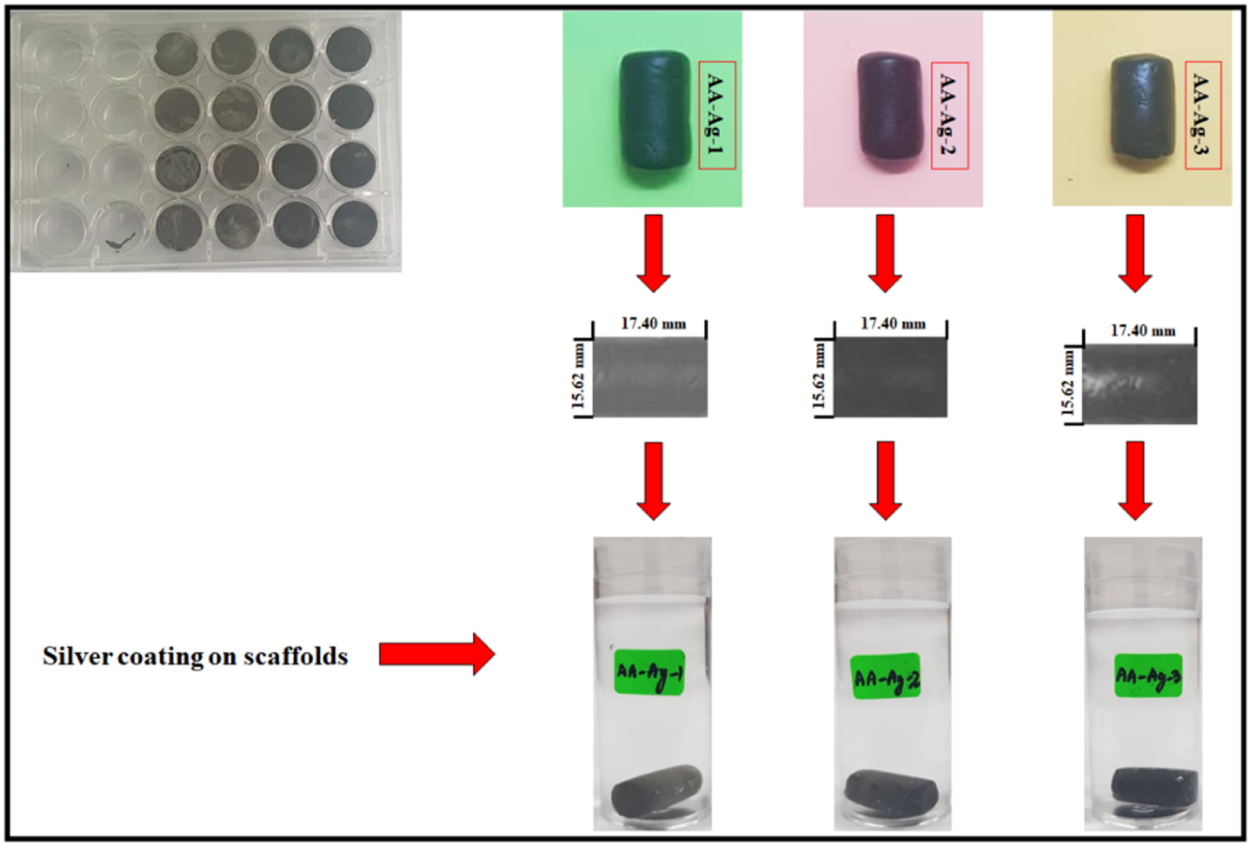

Figure 1. Silver coating over the polymeric nanocomposite scaffolds to enhance their antibacterial activates.

https://dx.doi.org/10.1021/acsomega.0c05596
ACS Omega 2021, 6, 4335−4346

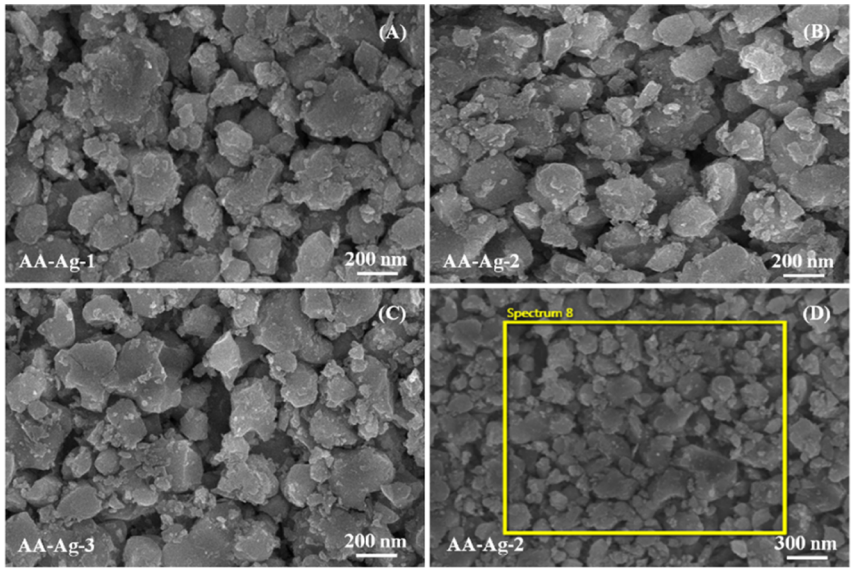

Element	Wt%	Wt% Sigma
C	6.19	4.66
O	39.11	2.12
P	16.16	0.86
Ca	35.11	1.82
Pd	1.11	0.21
Au	2.32	0.41
Total:	100	

Figure 2. Morphology of the synthesized particle sizes (A−C) of the polymeric nanocomposite through free radical polymerization via SEM. The polymeric nanocomposite material (AA-Ag-2) was selected for chemical composition analysis using SEM at 300 nm (D) and its EDX spectral profile (E) with percentage of elements (F).

The well-dried scaffolds were gold coated with a gold sputtering instrument before SEM and morphological analyses. The porosity and pore size were determined using the water displacement method. The wetting behavior of the scaffolds was recorded using a wetting analysis system (JY-82, Dingsheng, Chengde, China) to determine the hydrophobicity/hydrophilicity of scaffolds. The mechanical properties of the scaffolds were measured using a universal testing machine (Testometrics, United Kingdom) with a 5 mm/min loading rate. The obtained load−displacement data were used to draw strain−stress curves to analyze the mechanical behavior of the fabricated scaffolds.

2.2.2. Porosity. The porosity of the polymeric nanocomposite scaffolds was measured using the well-reported Jiang et al. method.[26] The dimensions of scaffolds such as diameter (d), height (h), and the dry weight (W_d) were measured carefully. The polymeric nanocomposite scaffolds were placed in ethanol for 5 min and the wet weight (W_w) was measured. The porosity percentage of the scaffolds was calculated using eq 1.

$$\text{Porosity}\ (\%) = \frac{W_w - W_d}{\rho\pi h(d/2)} \times 100 \quad (1)$$

where ρ is the ethanol density (0.789 g/cm^3), π is 3.1416, W_w is the weight of the wet scaffold, and W_d is the weight of the dried scaffold.

2.2.3. Swelling and Biodegradation. The swelling analysis of the scaffolds was conducted in aqueous and PBS solution (pH 7.4 at 37 °C). The dried scaffolds were cut into equal weight (50 mg) as the initial weight (W_i). These were soaked into a beaker (100 mL) of the corresponding solvent for 6 h. Then, the scaffolds were taken out of the media, blot dried using tissue paper, and the final weight (W_f) was recorded to calculate the swelling (%) using eq 2.

$$\text{Swelling}\ (\%) = \frac{W_f - W_i}{W_i} \times 100 \quad (2)$$

Biodegradation is an important propertyof biomaterial scaffolds after implantation; therefore, in vitro biodegradation was determined by immersing the scaffold in the PBS solution (pH 7.4 at 37 °C under 5% CO_2) for 1, 2, 3, 5, and 7 days (t). The weight loss of all the samples of scaffolds was determined using eq 3.

$$\text{Weight loss}\ (\%) = \frac{W_0 - W_t}{W_0} \times 100 \quad (3)$$

where W_0 is the initial weight of scaffolds and W_t is the weight of scaffolds at a time "t".

2.3. In Vitro Studies. *2.3.1. Antibacterial Activities.* The antibacterial activity of polymeric nanocomposite scaffolds was investigated against Gram +ive and Gram −ive bacteria (*E. coli*, *S. aureus*, and *P. aeruginosa*) using the agar disc diffusion method as reported by Valgas et al.[27] The molten agar was poured into the polystyrene culture plates and allowed to solidify at room temperature. Then, a sterilized glass spreader was used to spread bacterial strains over the solid agar uniformly. Approximately 80 mL of scaffold slurry was poured over each Petri dish and incubated at 37 °C for 24 h. The

https://dx.doi.org/10.1021/acsomega.0c05596
ACS Omega 2021, 6, 4335−4346

bacterial zone inhibition was measured (in mm) by CLSI disc diffusion breakpoints to analyze zone inhibition.[28]

2.3.2. Cell Culture and Morphological Analyses. The mouse preosteoblast cells were used to investigate biological activities against these polymeric scaffolds. The well-plates were coated with a 0.1% gelatin solution, and it was also taken as a positive control. Different polymeric composite scaffold concentrations were employed to evaluate cell culture and growth against *MC3T3-E1* cell lines. These cell culture plates were then incubated at at 37 °C with 5% CO_2 in α-MEM medium. Simultaneously, bovine fetal serum (10%) and Pen/Strep solutions were mixed to prepare α-MEM media. The cell morphology and cell culture were photographed using a Nikon ECLIPS TS100 fluorescence microscope, and a 488 nm excitation filter was used. Vital dye such as fluorescein diacetate (FDA, green color) was used to prevent scaffold extract microscopic background interference. A working solution from FDA stock in the serum-free medium was prepared and poured on the cells for 2 min to be absorbed by the cells. Later, these cells were rinsed with 1× saline phosphate solution to remove the extra FDA solvent from cells. Then, the morphology of the cell was captured using a Nikon ECLIPS TS100 fluorescence microscope.

2.3.3. Cell Viability and Cytotoxicity Using the NR Assay. The 12-well plates were used to seed the cells and the neutral red (NR) assay was used to determine cell viability and cytotoxicity for polymeric nanocomposite scaffolds. The *MC3T3-E1* cells (5000 cells) were used for every 24-well plates against different c concentrations of scaffold slurry (0.125−2.00 mg/mL) and incubated in a humid environment (95% humidity), 5% CO_2 at 37 °C for 24 h. The assay was conducted in triplicate, and each scaffold concentration was tested using the NR assay as reported by Repetto et al.[29] A destaining solution was employed for 10 min to destain these cells at 37 °C. Glacial acetic acid (1%), absolute ethanol (49%), and distilled water (50%) were mixed to prepare the destaining solution. PBS (150 μL) solution was used to wash plates, and then plates were immersed in the PBS solution. The washing solution was removed carefully by tapping plates. A microplate reader (Bio-Tek, ELx-800, USA) was used at 540 nm to record the optical density of the cell.

The percentage of cell viability was determined using eq 4.

$$\text{Cell viability (\%)} = \frac{OD_s}{OD_c} \times 100 \quad (4)$$

OD_s = OD of the sample, OD_c = OD of the control, and OD is optical density.

2.4. Statistical Analysis. The statistical data were interpreted using a statistical software framework (IBM, SPSS Statistics 21) to calculate the mean ± standard error (S.E.). These error bars are being presented as standard deviations ($p < 0.05$, $n = 3$) in results.

3. RESULTS AND DISCUSSION

3.1. SEM and EDX of Polymeric Nanocomposites. The morphology of all synthesized polymeric nanocomposite materials was observed at 100 nm by SEM as shown in the Figure 2A, 2B and 2C. The EDX spectral analysis with percentage elemental composition was performed as shown in Figure 2F before freeze-drying process.The SEM images (Figure 2A−C) demonstrate the individual particles comprised of ARX/nHAp/GO/AAc with an array of elongated particles of different sizes and shapes. The polymeric nanocomposite material exhibits an average particle size of 70 nm, with a minimum of 20 nm, as presented in Figure 2. These polymeric nanoparticles have different sizes because of different amounts of GO aggregates during the free-radical polymerization process. GO acts as a filler as well as a cross-linker because of different available O-based functional groups. These features of GO help control the size of polymeric nanocomposite materials that form aggregated because of extra cross-linking sites offered by GO.[30] The EDX analysis confirms the presence of C, O, P Ca Pd, and Au (Figures 1E,F) and the fabricated scaffolds contained only necessary elements without any contamination. In contrast, Pd and Au were present because of gold sputtering (Figure 2E,F).

3.2. FTIR Analysis. Figure 3 presents the FTIR spectra of polymeric nanocomposite scaffolds that show the functional

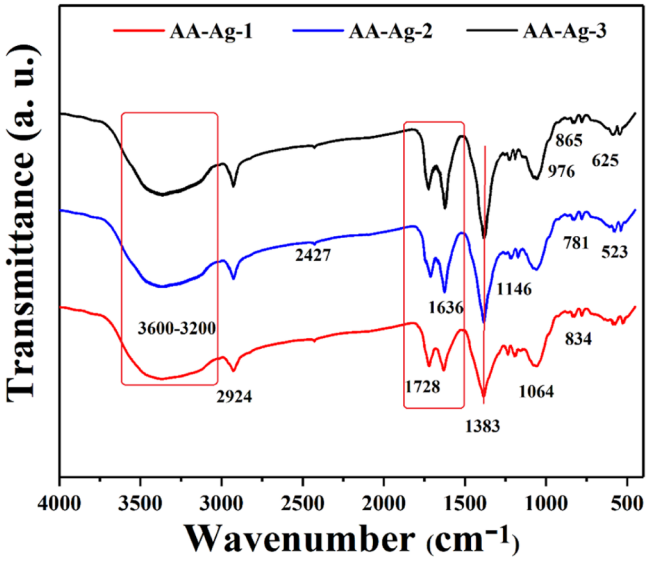

Figure 3. FTIR spectrum profile of all samples of scaffolds to determine different functional groups.

groups of the bioactive scaffolds through different vibrational peaks. The characteristic broadbands of polysaccharides at 3500−3200 and 1600 cm^{-1} are attributed to the stretching and bending vibrations of the hydrogen bond and hydroxyl (−OH) group, respectively.[31] The broadband 3500−3200 cm^{-1} presents the hydrogen bonding between arabinoxylan and AAc and the vibration peak at 2924 cm^{-1} is attributed to C−H. The grafting of arabinoxylan and AAc is confirmed by these vibration peaks.[32,33] The absorption peak at 2924 cm^{-1} is attributed to the stretching −CH group of the COOH groups and intramolecular bonding of O−H stretching of alcohols, respectively.[34,35] However, the absorption peaks at 2427 and 1728 cm^{-1} are attributed to the C═O stretching vibration. The peak intensity increases as the GO increases from AA-Ag-1 to AA-Ag-3 in the polymeric nanocomposite nanomaterials of a scaffold. The peaks at 1064 and 1383 cm^{-1} are attributed to cyclic and acyclic C−O stretching vibrations. The bands at 976 and 625 cm^{-1} are attributed to triply degenerated P−O stretching and O−P−O bending of nHAp and peaks at 625 and 523 cm^{-1} are attributed to the calcium phosphate (Ca^{2+} and PO_4^{3-}) moiety, respectively.[36] The peak from 700 to 400 cm^{-1} is attributed to n-Al_2O_3.[37] Moreover, the peak at 625 cm^{-1} confirms the presence of nHAp in the polymeric

https://dx.doi.org/10.1021/acsomega.0c05596
ACS Omega 2021, 6, 4335−4346

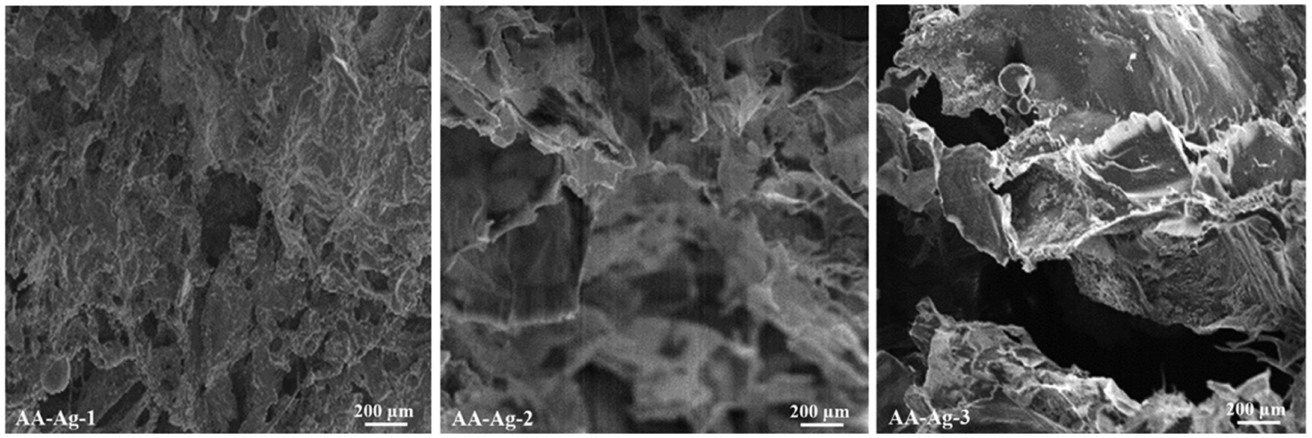

Figure 4. SEM images of the rough and porous scaffolds present the morphology of the polymeric nanocomposite scaffolds at 200 μm resolution.

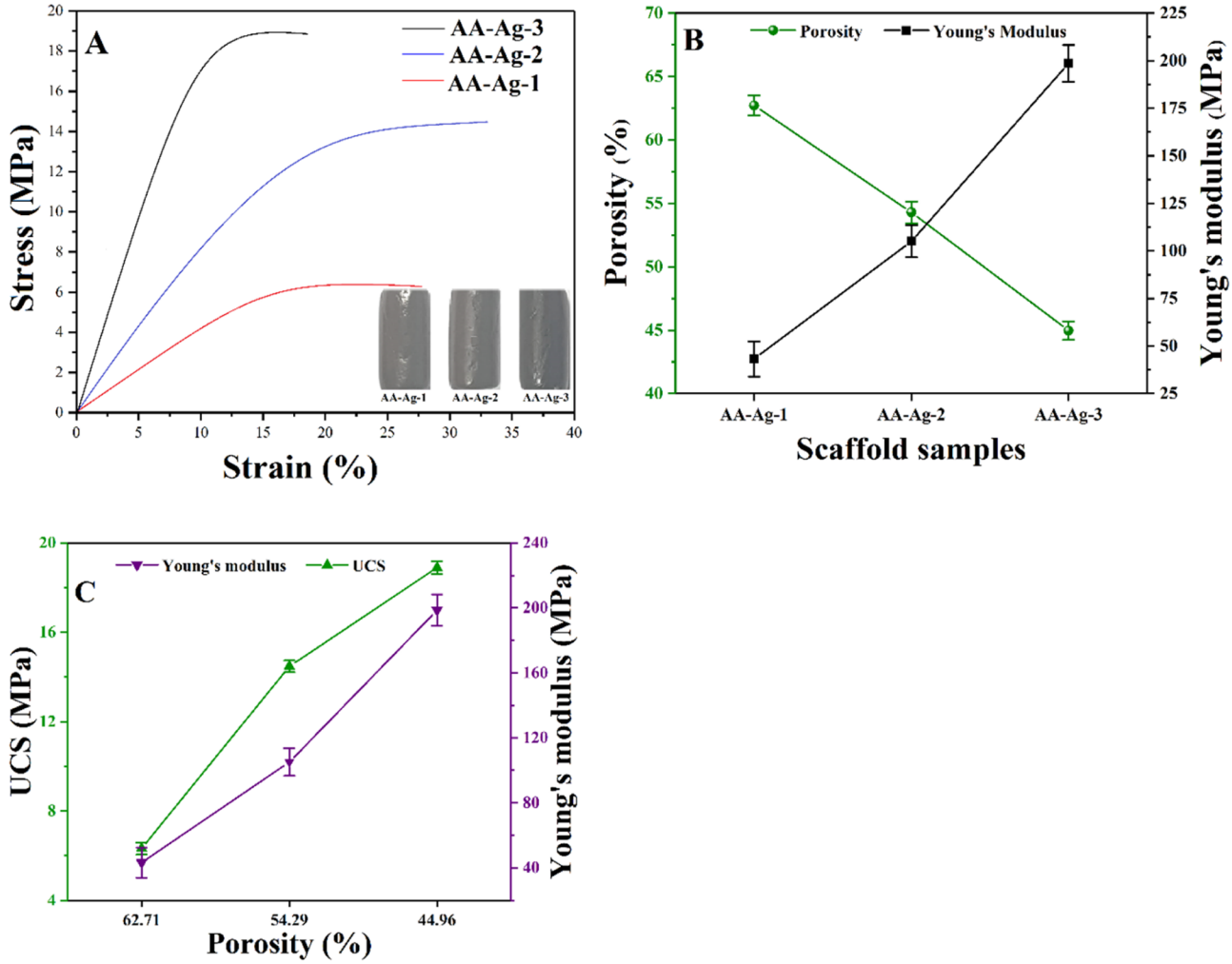

Figure 5. Mechanical and porous behavior of polymeric nanocomposite scaffolds has presented a (A) stress−strain curve, (B) shows the relationship of porosity (%) and Young's modulus, (C) presents the relationship of ultimate compression and Young's modulus.

nanocomposite scaffolds.[38] Hence, the spectra confirm the successful synthesis of polymeric nanocomposite material by exhibiting different absorption peaks.

3.3. SEM Analysis of Porous Scaffolds. The morphology of scaffolds has been investigated via SEM and presented in Figure 4. All scaffolds are highly porous with different pore sizes because of the variable amounts of GO. The polymeric nanocomposites have shown a well-interconnected structure, and the irregular pores are because of different amounts of absorbed water. The absorbed water on sublimation gives different pore shapes. The pore size of the scaffolds ranges from 300 to 400 μm.[15] The microporous morphologies of scaffolds are essential to facilitate cell growth and vascularization; these microstructures also help exchange gases (oxygen/

https://dx.doi.org/10.1021/acsomega.0c05596
ACS Omega 2021, 6, 4335−4346

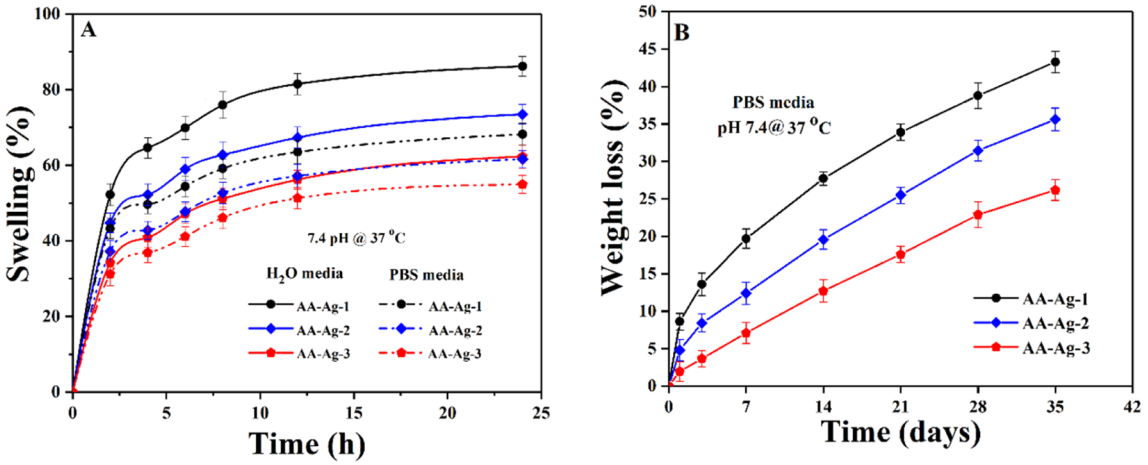

Figure 6. Swelling analysis of scaffolds (A) in different media (PBS solution and H_2O) with pH 7.4 at 37 °C. Degradation phenomena (B) in PBS solution under in vitro (pH 7.4 at 37 °C) conditions of all samples of scaffolds.

carbon dioxide), nutrients, and wastes. The morphology of polymeric nanocomposite scaffolds was observed at 200 μm to investigate the microstructure characteristics of the scaffolds. All scaffolds have supported the cell proliferation against the *MC3T3-E1* cell lines because of the porous morphology and the scaffold sample AA-Ag-2 was more bioactive and biocompatible. The optimized and uniformly distributed pore sizes encourage cell adherence, proliferation, and migration. These polymeric nanocomposite scaffolds also have increasing active sites and multifunctional characteristics because of GO, facilitating cell adherence that actively helps in osteogenesis.[39,40] Hence, the porous scaffold structures with a rough and different porous morphology confirm the successful fabrication of polymeric nanocomposite scaffolds and confirm the cross-linking behavior of GO.

3.4. Mechanical Properties and Porosity. Figure 5 presents the mechanical properties of the polymeric scaffolds, and it was observed an increasing amount of GO enhances the structural and mechanical characteristics.[41] The compression test was conducted to observe the mechanical properties of polymeric nanocomposite scaffolds, and it was found that an increasing amount of GO enhances the mechanical properties because of cross-linking behavior of GO. The mechanical testing of cylindrical scaffolds was performed to obtain a strain−stress curve, as shown in Figure 4A.[24] The Young's modulus of the porous scaffolds as a function of GO (a different amount) was calculated using the data obtained by the stress−strain curves. A relationship between Young's modulus and porosity percentage is presented in Figure 5A. There is a notable difference in the mechanical properties of AA-Ag-1, AA-Ag-2, and AA-Ag-3 because of the increasing amount of GO. The amount of GO increases the mechanical properties of the scaffolds. The Young's modulus and compressive strength of the AA-Ag-1, AA-Ag-2, and AA-Ag-3 scaffolds are 43.26, 105.08, and 198.61, and 6.32, 14.47, and 18.89 MPa, respectively. These results indicate that the increasing amount of GO improved the mechanical properties of scaffolds. The uniform and homogeneous dispersion of nanofillers (nHAp, Al_2O_3, and GO) into the polymeric matrix enhances mechanical properties. These filers have a larger surface area with a higher surface energy. GO contains numerous oxygen-based functional groups such as a basal plane with epoxy and hydroxyl groups and on the GO edges, carboxylic and carbonyl groups are located.[24,42] These characteristics facilitate the interaction of fillers with the polymeric matrix via van der Waals forces, hydrogen bonding, or other interactions to provide substantial adhesion with the polymeric matrix.[43] nHAp, nAl_2O_3, and GO-sheets were mixed homogeneously to achieve appropriate adhesion with the polymeric matrix that reinforces the polymeric nanocomposite scaffolds.[24,44] Different amounts of GO in the polymeric nanocomposite scaffolds have different chemical structures that affect the interface grain matrix. These scaffolds with different mechanical behaviors can be used to heal fractured bones with different load-bearing.

Moreover, HAp supports the microstructure significantly, and the optimum amount of GO improves the mechanical strength, grain size, and grain boundary properties. The pore size is directly related to the surface area and a smaller pore size has a high surface area. The smaller size of the pores increases the interaction with neighboring grain, thereby improving mechanical properties,[45] as shown in Figure 5B,C. Hence, the optimum porosity and pore size encourage cell adherence and migration and control mechanical properties.

Figure 5B,C presents the porosity results and its relationship with mechanical strength for polymeric nanocomposite scaffolds (AA-Ag-1, AA-Ag-2, and AA-Ag-3). The material composition and GO amounts have altered the porosity and pore area of the polymeric nanocomposite scaffolds.[46] Figure 5B. By increasing the amount of GO, with no change in nHAp, n-Al_2O_3 and silver solution concentration, a decrease in porosity was observed because of the crosslinking nature of GO that holds the microstructure tightly, as shown in figures 5B and 5C. AA-Ag-1 has maximum porosity, while AA-Ag-3 has the least porosity. It is estimated that distinctive pore sizes and porosities of the scaffolds are caused by the addition of different GO quantities that can influence their mechanical properties. The stress−strain curves in Figure 5A, analysis of mechanical and porosity features as in Figure 5B, and porosity relationship in Figure 5C) are presenting a unique relationship between mechanical strength and porosity. These polymeric nanocomposite scaffolds exhibited typical sequential elastic regions leading to a decrease in the slope region, which gradually decreased as scaffold porosity decreased (Figure 5A). A decrease in mechanical strength resulted from an increase in (Figure 5C) porosity from AA-Ag-1 to AA-Ag-3 for GO.

https://dx.doi.org/10.1021/acsomega.0c05596
ACS Omega 2021, 6, 4335−4346

Hence, it was observed that an increasing amount of GO decreases the porosity and increases mechanical behavior. These fabricated scaffolds can be used for different load-bearing applications in bone tissue engineering.

3.5. Swelling and Biodegradation. The scaffolds' swelling properties were studied under standard in vitro (pH 7.4 at 37 °C) conditions in PBS buffer and aqueous media. Figure 6A presents that scaffolds' swelling behavior was found to be different in both media with different amounts of GO. The swelling of scaffolds is less in PBS media and more in aqueous media because of different physicochemical properties and interaction of different available functions with the media. The scaffolds contain mostly alcoholic and carboxylic acid functional groups. The swelling of scaffolds is a vital property that helps osteogenesis by facilitating cell adherence and proliferation. During swelling, the porosity and pore size of scaffolds increase, facilitating cell migration to support cell growth and other cellular activities.[47] The maximum swelling of AA-Ag-3 has more functionalities because of more amounts of GO and AA-Ag-1 show less swelling because of less amounts of GO and ultimately has fewer functionalities. Hence, the increasing functionalities facilitate hydrogen bonding and the increasing amount of GO causes more swelling.

The biodegradability of scaffolds was carried out in the PBS buffer solution under in vitro (pH 7.4 at 37 °C) conditions to determine the better formulation of scaffolds. The biodegradation supports osteogenesis and the scaffolds offer uniform degradation through weight loss. The biodegradation of scaffolds as a function of time is shown in Figure 6B. Different biodegradation rates are because of the different GO amounts that play a role in swelling and biodegradation. The increasing amount of GO facilitates more cross-linking because of increasing functionalities into polymeric scaffolds that control swelling and biodegradation. Biodegradation was found to be in the order of AA-Ag-3> AA-Ag-2> AA-Ag-1. Hence, it is evident from the results that an increasing amount of GO has an inverse effect on swelling and a direct effect on biodegradation that confirm the nature of GO as a cross-linker. It holds the materials and matrix closer that controls swelling and degradation.

3.6. In Vitro Analysis. *3.6.1. Antibacterial Activities.* The antibacterial activities of polymeric nanocomposite scaffolds (AA-Ag-1, AA-Ag-2, and AA-Ag-3) are shown in Figure 7 against *E. coli*, *P. aeruginosa* (Gram −ive), and *S. aureus* (Gram +ive) bacterial strains. The antibacterial inhibition zones were measured for every sample. It was found that AA-Ag-3 shows maximum antibacterial activities in terms of zone antibacterial bacterial activity and AA-Ag-3 shows the least among all samples. The bacterial cell membrane is composed of lipopolysaccharides and phospholipids. The bacterial population increases through binary fission through transcription and translation.[48] Because polymeric nanocomposite materials contain biopolymers, nHAp, n-Al_2O_3, and GO, these the biopolymers induce their charge into the bacterial membrane and take over the control of bacterial DNA to hinder transcription and translation. The sharp edges of GO puncture the cellular membrane to destroy the bacterial structure. The silver nanoparticles penetrate the bacterial membrane as well by destroying the bacterial membrane. The polymeric part of scaffolds enters through the punctured membrane to take control over DNA and hinder bacterial activities and populations. It can also be explained that the polymeric matrix of the nanocomposite scaffolds may also interact with lipopolysaccharides and phospholipids that induce charges that kill bacteria. Hence, AA-Ag-3 presented the highest antimicrobial activities because of the maximum amount of GO that interacts with the bacterial membrane and DNA to control bacterial growth.[49] The enhanced antibacterial characteristics of silver-coated scaffold materials are because of the synergistic effect of the GO and Ag^+ system. GO is a sheet-like material that contains several oxygen-based functional groups, a π-conjugated structure, a larger specific surface area, negatively charged, and so forth and because of these characteristics GO can easily interact with the bacterial membrane through hydrogen bonding, van der Waals forces, and other electrostatic and $\pi-\pi$ interactions.[24,50] The sharp edges of GO rupture the bacterial cytomembrane by adsorbing, wrapping, and capturing effects and attract more Ag^+ over the GO-sheet because of highly negative charge density that effectively enhances antibacterial activities.[24] Because of the oxidation of Ag by water/oxygen, it produces Ag^+ and ROS, both may attack the DNA to inhibit replication.[43,51] It can be explained that the polymeric part of the scaffold may penetrate the bacterial cytomembrane to take control of DNA to inhibit bacterial growth.[52] Hence, it is confirmed that GO, Ag, and polymeric matrix all together enhanced the antibacterial activities.

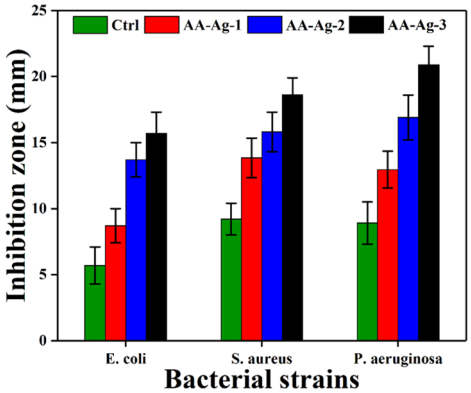

Figure 7. Antibacterial activity of polymeric nanocomposite scaffolds against Gram +ive and Gram −ive bacterial strains and zones of inhibition were determined in mm.

3.6.2. Cell Morphology. Figure 8 shows different behaviors of *MC3T3-E1* cell lines against polymeric nanocomposite scaffolds. The wells of cell culture plates were coated with gelatin to enhance cell attachment. These plates were incubated for 48 and 72 h under standard in vitro conditions to analyze cell growth and morphology. These polymeric nanocomposite scaffolds have encouraged the growth of *MC3T3-E1* cell lines. Initially, the cell morphology is not mature and looks like a thin thread-like morphology (yellow arrow) and the mature growth with a proper cylindrical shape occurs after 48 h. After 72 h, the cell morphology became cylindrical spreading and covering more scaffold surface and showing proper cell adherence. The scaffold (AA-Ag-3) has shown a well cylindrical and adhered shape compared to the scaffold (AA-Ag-1). The change in the cell morphology may be because of the increasing amount of GO that enhances material multifunctionality, which encourages cell adherence and allows interaction of materials and cellular membranes.[53] The yellow arrows represent the thread-like cell morphology and the red arrow represents the proper cylindrical shape of

https://dx.doi.org/10.1021/acsomega.0c05596
ACS Omega 2021, 6, 4335−4346

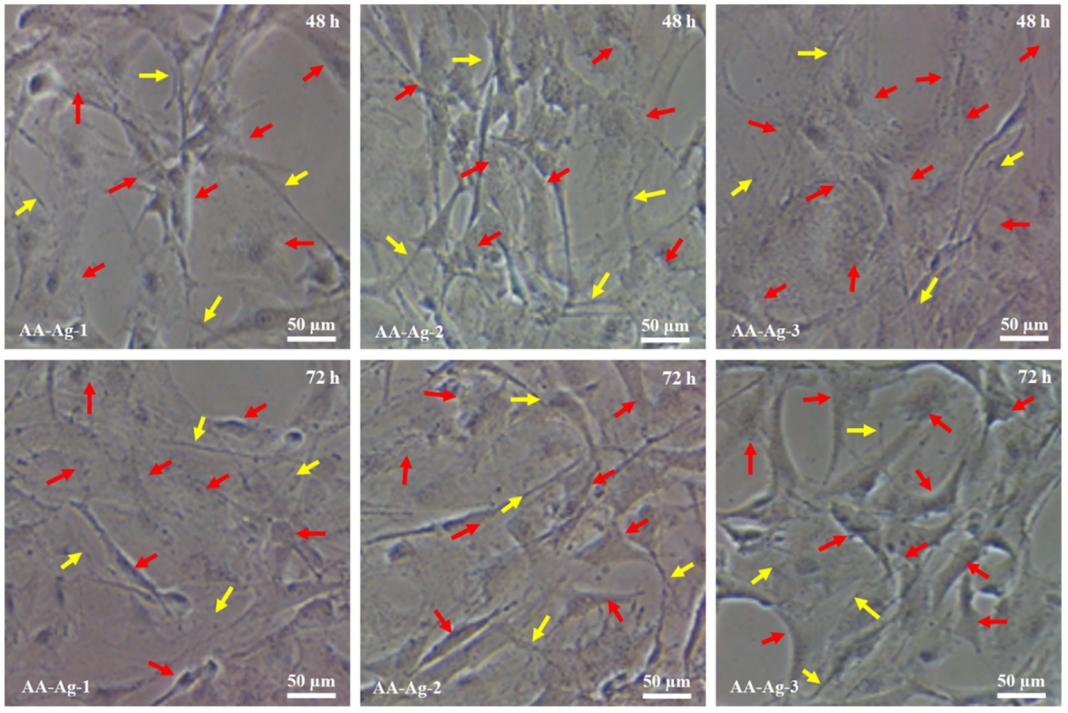

Figure 8. The cell morphology of polymeric nanocomposite scaffolds against mouse preosteoblast (*MC3T3-E1*) cell lines after 48 and 72 h. The yellow arrows represent the thread-like morphology, and red arrows represent cylindrical and mature morphology.

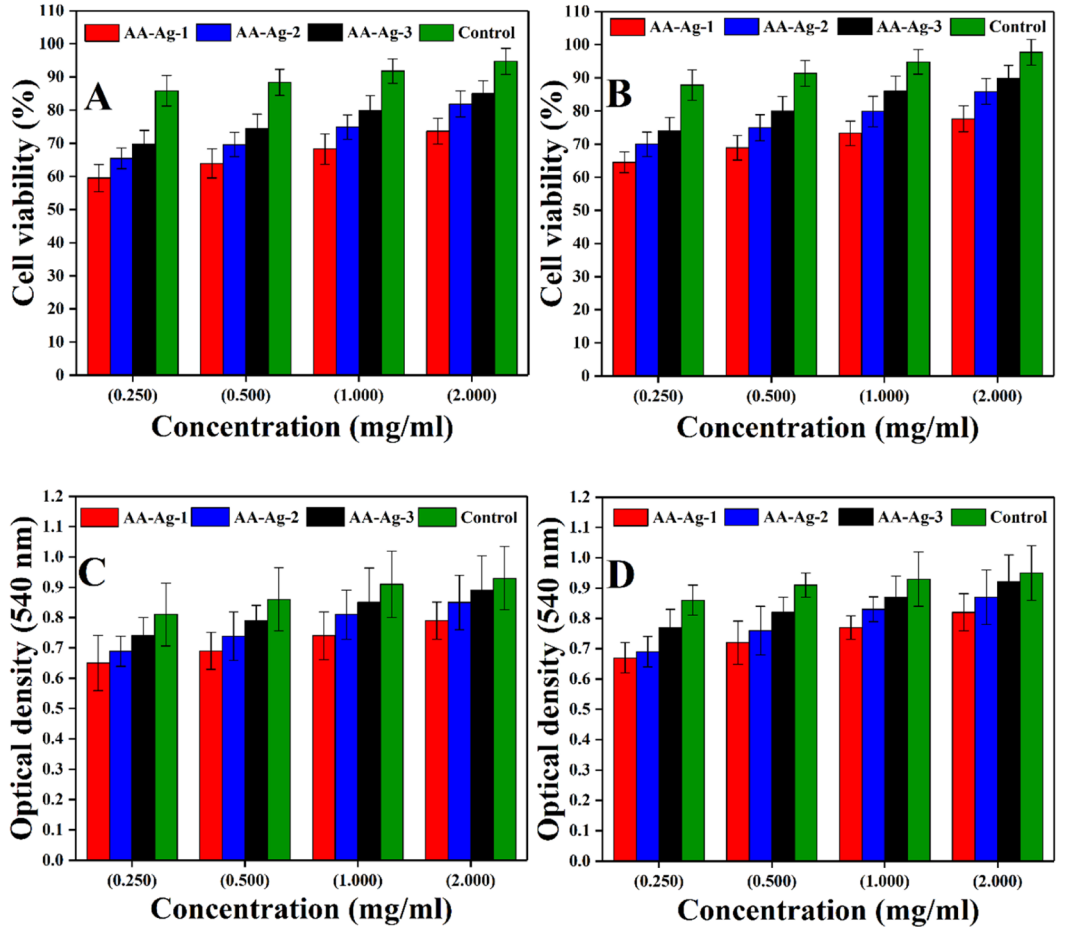

Figure 9. Cell viability (A,C) and optical density (B,D) of all polymeric nanocomposite scaffolds against the *MC3T3-E1* cell line at various concentrations (0.250, 0.500, 1.000, and 2.000 mg/mL) after different intervals (48 and 72 h) along with positive controls.

https://dx.doi.org/10.1021/acsomega.0c05596
ACS Omega 2021, 6, 4335−4346

the cells. An increasing amount of GO means increasing multifunctional properties of the polymeric nanocomposite scaffolds. It helps cell proliferation and cell culture and polymeric nanocomposite scaffold extracts support better cell growth by retaining their cell morphology.[54]

All these scaffolds provide an encouraging microenvironment for cell adherence that supports cell proliferation. It was observed that AA-Ag-3 encourages more cell adherence than other samples. It confirms the biocompatible behavior of these scaffolds. The increasing time encourages more cell adherence, and flatter cell morphology was observed after 72 h by covering a wider area. Hence, AA-Ag-3 provides a better microenvironment for cell adherence and proliferation, which was attributed to cell adherence factors. The increasing amount of GO increases the surface functional properties because of different available functional groups (COO^- and OH^-), facilitating cell adherence through hydrogen bonding.[55,56] The increasing amount of GO increases the surface charge density of scaffolds, increasing the interaction of the cellular membrane with the surface of the scaffold that encourages more cell adherence.[57] The homogenized dispersion of ceramic materials (nHAp and nAl_2O_3) and the filler (GO) provides active sites for cell adherence. Hence, increasing GO increases surface functionalities that support more cell adherence and proliferation to regenerate new tissue to heal fractured bone.

3.6.3. Cell Viability and Optical Density. .Bone healing with scaffoled implanation is a multiple step process. Cell adherence is an important step that arises because of the interaction between cell and the material surface, leading to the formation of new tissue to repair or regenerate new bone tissue. The multifunctional surface encouraging cell adherence to the scaffold matrix is a vital bone formation step. These polymeric nanocomposite scaffolds have potential cell adhesion against the *MC3T3-E1* cell lines. All samples have exhibited low cytotoxicity by retaining an appropriate cell morphology compared to the control, as shown in Figure 9A,B. The minor differences in cell viability may be because of the physicochemical behavior of these scaffolds due to different GO amounts.[53] It was observed that AA-Ag-3 had exhibited maximum cell viability, which is very close to positive control and AA-Ag-1 has the least cell viability. The optical density of these follows a similar trend to cell viability. AA-Ag-3 has a maximum optical density as compared to AA-Ag-1 and very close to the positive control. Hence, it was observed that increasing amount of GO increases functionalities in the polymeric nanocomposite scaffolds because of multifunctional groups. The increasing amount of GO also increases cell densities, as shown in Figure 9C,D. These functionalities interact with the cell membrane to facilitate their adherence, proliferation, and migration.

4. CONCLUSIONS

In this study, polymeric nanocomposite materials were synthesized using various amounts of GO to fabricate porous scaffolds and coated with silver nanoparticles to enhance biomechanical properties and antibacterial function. Different GO sheets with a constant amount of nHAp, n-Al_2O_3, and alumina were loaded into the polymeric (ARX-*co*-AAc) matrix. The porous scaffolds exhibited an improved therapeutic impact of physicochemical, biomechanical, and antibacterial properties as the amount of GO increased. Moreover, the porous morphology, swelling, and biodegradation with enhanced biological properties were observed because of additional cross-linking of GO with increased antibacterial activities. Furthermore, the AA-Ag-3 scaffold demonstrated excellent biocompatibility and cell morphology without affecting cell adhesion, viability, and proliferation. Consequently, these porous scaffolds have excellent potential in bone tissue engineering.

AUTHOR INFORMATION

Corresponding Authors

Saiful Izwan Abd Razak − *School of Biomedical Engineering and Health Sciences, Faculty of Engineering and Center for Advanced Composite Materials, Universiti Teknologi Malaysia, 81300 Skudai, Malaysia*; Email: saifulizwan@utm.my

Rashid Amin − *Department of Biology, College of Sciences, University of Hafr Al Batin, 39524 Hafar Al-batin, Saudi Arabia*; orcid.org/0000-0003-4627-7147; Email: rashida@uhb.edu.sa

Authors

Muhammad Umar Aslam Khan − *School of Biomedical Engineering and Health Sciences, Faculty of Engineering, Universiti Teknologi Malaysia, 81300 Skudai, Malaysia; Department of Metallurgical and Materials Engineering, University of the Punjab, 54590 Lahore, Pakistan; Institute for Personalized Medicine, School of Biomedical Engineering, Shanghai Jiao Tong University, 200030 Shanghai, China*

Hassan Mehboob − *Department of Engineering Management, College of Engineering, Prince Sultan University, Riyadh 11586, Saudi Arabia*

Mohammed Rafiq Abdul Kadir − *School of Biomedical Engineering and Health Sciences, Faculty of Engineering, Universiti Teknologi Malaysia, 81300 Skudai, Malaysia*

T. Joseph Sahaya Anand − *Sustainable and Responsive Manufacturing Group, Faculty of Mechanical and Manufacturing Engineering Technology, Universiti Teknikal Malaysia Melaka, 76100 Melaka, Malaysia*

Fawad Inam − *Department of Engineering and Computing, University of East London, E16 2RD London, U.K.*

Saqlain A. Shah − *Nanotechnology Lab, Department of Physics, Forman Christian College (University), 54600 Lahore, Pakistan*

Mahmoud E. F. Abdel-Haliem − *Botany and Microbiology Department, Faculty of Science, Zagazig University, 44519 Zagazig, Egypt; Department of Biology, College of Sciences, University of Hafr Al Batin, 39524 Hafar Al-batin, Saudi Arabia*

Complete contact information is available at: https://pubs.acs.org/10.1021/acsomega.0c05596

Author Contributions

M.U.A.K. and S.I.A.R. conceptualized the work; M.U.A.K. and S.I.A.R. contributed in data curation; M.U.A.K. and F.I. contributed in formal analysis; H.M., S.I.A.R. and M.R.A.K. helped in funding acquisition; S.A.S., S.I.A.R. and M.R.A.K. helped in investigation; M.U.A.K. and S.A.S. helped in methodology;S.A.S., S.I.A.R., M.R.A.K., and R.A. helped in project administration; M.R.A.K., S.I.A.R., and T.J.S.A. contributed in resource acquisition; M.U.A.K., H.M., and F.I. helped in software-related work; M.R.A.K., S.A.S., and S.I.A.R. supervised the work; S.A.S. and F.I. validated the work; M.U.A.K. and H.M. contributed in visualization; M.U.A.K.

https://dx.doi.org/10.1021/acsomega.0c05596
ACS Omega 2021, 6, 4335−4346

contributed in writing the original draft; and M.U.A.K., R.A., and M.E.F.A.-H contributed in writing—review and editing.

Notes

The authors declare no competing financial interest.

■ ACKNOWLEDGMENTS

We want to acknowledge Universiti Teknologi Malaysia for the financial support through Universiti Teknologi Malaysia research grants (02M44) and seed project# SEED-PSU-23-12-2019 and like to acknowledge the support of Prince Sultan University by paying the Article Processing Charges (APC) of this publication and also thank the support of Structures and Materials lab at Prince Sultan University, Saudi Arabia.

■ REFERENCES

(1) Rosellini, E.; Zhang, Y. S.; Migliori, B.; Barbani, N.; Lazzeri, L.; Shin, S. R.; Dokmeci, M. R.; Cascone, M. G. Protein/polysaccharide-based scaffolds mimicking native extracellular matrix for cardiac tissue engineering applications. *J. Biomed. Mater. Res., Part A* **2018**, *106*, 769−781.

(2) Griffith, L. G.; Naughton, G. Tissue engineering–current challenges and expanding opportunities. *Sci* **2002**, *295*, 1009−1014.

(3) Bassas-Galia, M.; Follonier, S.; Pusnik, M.; Zinn, M. Natural Polymers: A Source of Inspiration. In *Bioresorbable polymers for biomedical applications, From Fundamentals to Translational Medicine*; Perale, G., Hilborn, J., Eds.; Woodhead Publishing, 2017; pp 31−64.

(4) Patil, S.; Singh, N. Antibacterial silk fibroin scaffolds with green synthesized silver nanoparticles for osteoblast proliferation and human mesenchymal stem cell differentiation. *Colloids Surf., B* **2019**, *176*, 150−155.

(5) Kiran, A. S. K.; Sampath Kumar, T. S.; Perumal, G.; Sanghavi, R.; Doble, M.; Ramakrishna, S. Dual nanofibrous bioactive coating and antimicrobial surface treatment for infection resistant titanium implants. *Prog. Org. Coat.* **2018**, *121*, 112−119.

(6) Ai, J.; Kiasat-Dolatabadi, A.; Ebrahimi-Barough, S.; Ai, A.; Lotfibakhshaiesh, N.; Norouzi-Javidan, A.; Saberi, H.; Arjmand, B.; Aghayan, H. R. Polymeric scaffolds in neural tissue engineering: a review. *Arch. Neurosci.* **2014**, *1*, 15−20.

(7) Haghdadeh, P.; Ghaffari, M.; Ramezanzadeh, B.; Bahlakeh, G.; Saeb, M. R. The role of functionalized graphene oxide on the mechanical and anti-corrosion properties of polyurethane coating. *J. Taiwan Inst. Chem. Eng.* **2018**, *86*, 199−212.

(8) Shuai, C.; Feng, P.; Gao, C.; Shuai, X.; Xiao, T.; Peng, S. Graphene oxide reinforced poly (vinyl alcohol): nanocomposite scaffolds for tissue engineering applications. *RSC Adv.* **2015**, *5*, 25416−25423.

(9) Gao, Y.; Shao, W.; Qian, W.; He, J.; Zhou, Y.; Qi, K.; Wang, L.; Cui, S.; Wang, R. Biomineralized poly (l-lactic-co-glycolic acid)-tussah silk fibroin nanofiber fabric with hierarchical architecture as a scaffold for bone tissue engineering. *Mater. Sci. Eng., C* **2018**, *84*, 195−207.

(10) Khan, M. U. A.; Al-Thebaiti, M. A.; Hashmi, M. U.; Aftab, S.; Abd Razak, S. I.; Abu Hassan, S.; Abdul Kadir, M. R.; Amin, R. Synthesis of Silver-Coated Bioactive Nanocomposite Scaffolds Based on Grafted Beta-Glucan/Hydroxyapatite via Freeze-Drying Method: Anti-Microbial and Biocompatibility Evaluation for Bone Tissue Engineering. *Mater* **2020**, *13*, 971.

(11) Shuai, C.; Guo, W.; Gao, C.; Yang, Y.; Xu, Y.; Liu, L.; Qin, T.; Sun, H.; Yang, S.; Feng, P. Calcium silicate improved bioactivity and mechanical properties of poly (3-hydroxybutyrate-co-3-hydroxyvalerate) scaffolds. *Polymers* **2017**, *9*, 175.

(12) Benhacine, F.; Hadj-Hamou, A. s.; Habi, A. Development of long-term antimicrobial poly (ϵ-caprolactone)/silver exchanged montmorillonite nanocomposite films with silver ion release property for active packaging use. *Polym. Bull.* **2016**, *73*, 1207−1227.

(13) Qian, L.; Zhang, H. Controlled freezing and freeze drying: a versatile route for porous and micro-/nano-structured materials. *J. Chem. Technol. Biotechnol.* **2011**, *86*, 172−184.

(14) Discher, D. E.; Mooney, D. J.; Zandstra, P. W. Growth factors, matrices, and forces combine and control stem cells. *Sci* **2009**, *324*, 1673−1677.

(15) Aslam Khan, M. U.; Mehboob, H.; Abd Razak, S. I.; Yahya, M. Y.; Mohd Yusof, A. H.; Ramlee, M. H.; Sahaya Anand, T. J.; Hassan, R.; Aziz, A.; Amin, R. Development of Polymeric Nanocomposite (Xyloglucan-co-Methacrylic Acid/Hydroxyapatite/SiO2) Scaffold for Bone Tissue Engineering Applications—In-Vitro Antibacterial, Cytotoxicity and Cell Culture Evaluation. *Polymers* **2020**, *12*, 1238.

(16) Khan, M. U. A.; Haider, S.; Shah, S. A.; Razak, S. I. A.; Hassan, S. A.; Kadir, M. R. A.; Haider, A. Arabinoxylan-co-AA/HAp/TiO2 nanocomposite scaffold a potential material for bone tissue engineering: An in vitro study. *Int. J. Biol. Macromol.* **2020**, *151*, 584−594.

(17) Khan, M. U. A.; Haider, S.; Haider, A.; Kadir, M. R. A.; Abd Razak, S. I.; Shah, S. A.; Javad, A.; Shakir, I.; Al-Zahrani, A. A. Development of Porous, Antibacterial and Biocompatible GO/n-HAp/Bacterial Cellulose/β-Glucan Biocomposite Scaffold for Bone Tissue Engineering. *Arabian J. Chem.* **2020**, *14*, 102924.

(18) Broekaert, W. F.; Courtin, C. M.; Verbeke, K.; Van de Wiele, T.; Verstraete, W.; Delcour, J. A. Prebiotic and other health-related effects of cereal-derived arabinoxylans, arabinoxylan-oligosaccharides, and xylooligosaccharides. *Crit. Rev. Food Sci. Nutr.* **2011**, *51*, 178−194.

(19) Saghir, S.; Iqbal, M. S.; Koschella, A.; Heinze, T. Ethylation of arabinoxylan from Ispaghula (Plantago ovata) seed husk. *Carbohydr. Polym.* **2009**, *77*, 125−130.

(20) Khan, M. U. A.; Raza, M. A.; Razak, S. I. A.; Abdul Kadir, M. R.; Haider, A.; Shah, S. A.; Mohd Yusof, A. H.; Haider, S.; Shakir, I.; Aftab, S. Novel Functional Antimicrobial and Biocompatible Arabinoxylan/Guargum Hydrogel for Skin Wound Dressing Applications. *J. Tissue Eng. Regener. Med.* **2020**, *14*, 1488−1501.

(21) Dey, R. E.; Zhong, X.; Youle, P. J.; Wang, Q. G.; Wimpenny, I.; Downes, S.; Hoyland, J. A.; Watts, D. C.; Gough, J. E.; Budd, P. M. Synthesis and Characterization of Poly (vinylphosphonic acid-co-acrylic acid) Copolymers for Application in Bone Tissue Scaffolds. *Macromolecules* **2016**, *49*, 2656−2662.

(22) Shuai, C.; Yang, W.; Feng, P.; Peng, S.; Pan, H. Accelerated degradation of HAP/PLLA bone scaffold by PGA blending facilitates bioactivity and osteoconductivity. *Bioact. Mater.* **2021**, *6*, 490−502.

(23) Ghauri, F. A.; Raza, M. A.; Baig, M. S.; Ibrahim, S. Corrosion study of the graphene oxide and reduced graphene oxide-based epoxy coatings. *Mater. Res. Express* **2017**, *4*, 125601.

(24) Shuai, C.; Guo, W.; Wu, P.; Yang, W.; Hu, S.; Xia, Y.; Feng, P. A graphene oxide-Ag co-dispersing nanosystem: dual synergistic effects on antibacterial activities and mechanical properties of polymer scaffolds. *Chem. Eng. J.* **2018**, *347*, 322−333.

(25) Saghir, S.; Iqbal, M. S.; Hussain, M. A.; Koschella, A.; Heinze, T. Structure characterization and carboxymethylation of arabinoxylan isolated from Ispaghula (Plantago ovata) seed husk. *Carbohydr. Polym.* **2008**, *74*, 309−317.

(26) Jiang, L.; Li, Y.; Xiong, C.; Su, S.; Ding, H. Preparation and properties of bamboo fiber/nano-hydroxyapatite/poly (lactic-co-glycolic) composite scaffold for bone tissue engineering. *ACS Appl. Mater. Interfaces* **2017**, *9*, 4890−4897.

(27) Valgas, C.; Souza, S. M. d.; Smânia, E. F. A.; Smânia, A., Jr. Screening methods to determine antibacterial activity of natural products. *Braz. J. Microbiol.* **2007**, *38*, 369−380.

(28) Simons, C.; Walsh, S. E.; Maillard, J.-Y.; Russell, A. D. A note: ortho-phthalaldehyde: proposed mechanism of action of a new antimicrobial agent. *Lett. Appl. Microbiol.* **2000**, *31*, 299−302.

(29) Repetto, G.; Del Peso, A.; Zurita, J. L. Neutral red uptake assay for the estimation of cell viability/cytotoxicity. *Nat. Protoc.* **2008**, *3*, 1125.

(30) Qin, Y.; Yuan, J.; Li, J.; Chen, D.; Kong, Y.; Chu, F.; Tao, Y.; Liu, M. Crosslinking Graphene Oxide into Robust 3D Porous N-Doped Graphene. *Adv. Mater.* **2015**, *27*, 5171−5175.

(31) Kamal, H.; Abd-Elrahim, F. M.; Lotfy, S. Characterization and some properties of cellulose acetate-co-polyethylene oxide blends

https://dx.doi.org/10.1021/acsomega.0c05596
ACS Omega 2021, 6, 4335−4346

prepared by the use of gamma irradiation. *J. Radiat. Res. Appl. Sci.* **2014**, *7*, 146−153.
(32) Mansur, H. S.; de S. Costa, E., Jr; Mansur, A. A. P.; Barbosa-Stancioli, E. F. Cytocompatibility evaluation in cell-culture systems of chemically crosslinked chitosan/PVA hydrogels. *Mater. Sci. Eng., C* **2009**, *29*, 1574−1583.
(33) Srivastava, A.; Kumar, R. Synthesis and characterization of acrylic acid-g-(-carrageenan) copolymer and study of its application. *Int. J. Carbohydr. Chem.* **2013**, *2013*, 892615.
(34) Szabó, T.; Berkesi, O.; Dékány, I. DRIFT study of deuterium-exchanged graphite oxide. *Carbon* **2005**, *43*, 3186−3189.
(35) Muruganandi, G.; Saravanan, M.; Vinitha, G.; Jessie Raj, M. B.; Sabari Girisun, T. C. Barium borate nanorod decorated reduced graphene oxide for optical power limiting applications. *Opt. Mater.* **2018**, *75*, 612−618.
(36) Destainville, A.; Champion, E.; Bernache-Assollant, D.; Laborde, E. Synthesis, characterization and thermal behavior of apatitic tricalcium phosphate. *Mater. Chem. Phys.* **2003**, *80*, 269−277.
(37) Djebaili, K.; Mekhalif, Z.; Boumaza, A.; Djelloul, A. XPS, FTIR, EDX, and XRD analysis of Al2O3 scales grown on PM2000 alloy. *J. Spectrosc.* **2015**, *2015*, 1−16.
(38) Abd-Khorsand, S.; Saber-Samandari, S.; Saber-Samandari, S. Development of nanocomposite scaffolds based on TiO2 doped in grafted chitosan/hydroxyapatite by freeze drying method and evaluation of biocompatibility. *Int. J. Biol. Macromol.* **2017**, *101*, 51−58.
(39) Caló, E.; Khutoryanskiy, V. V. Biomedical applications of hydrogels: A review of patents and commercial products. *Eur. Polym. J.* **2015**, *65*, 252−267.
(40) Karahaliloglu, Z.; Kilicay, E.; Denkbas, E. B. Antibacterial chitosan/silk sericin 3D porous scaffolds as a wound dressing material. *Artif. Cells, Nanomed., Biotechnol.* **2017**, *45*, 1172−1185.
(41) Pang, W.; Ni, Z.; Chen, G.; Huang, G.; Huang, H.; Zhao, Y. Mechanical and thermal properties of graphene oxide/ultrahigh molecular weight polyethylene nanocomposites. *RSC Adv.* **2015**, *5*, 63063−63072.
(42) Al-Arjan, W. S.; Aslam Khan, M. U.; Nazir, S.; Abd Razak, S. I.; Abdul Kadir, M. R. Development of Arabinoxylan-Reinforced Apple Pectin/Graphene Oxide/Nano-Hydroxyapatite Based Nanocomposite Scaffolds with Controlled Release of Drug for Bone Tissue Engineering: In-Vitro Evaluation of Biocompatibility and Cytotoxicity against MC3T3-E1. *Coatings* **2020**, *10*, 1120.
(43) Guo, W.; Liu, W.; Xu, L.; Feng, P.; Zhang, Y.; Yang, W.; Shuai, C. Halloysite nanotubes loaded with nano silver for the sustained-release of antibacterial polymer nanocomposite scaffolds. *J. Mater. Sci. Technol.* **2020**, *46*, 237−247.
(44) Khan, M. U. A.; Raza, M. A.; Mehboob, H.; Kadir, M. R. A.; Abd Razak, S. I.; Shah, S. A.; Iqbal, M. Z.; Amin, R. Development and in vitro evaluation of κ-carrageenan based polymeric hybrid nanocomposite scaffolds for bone tissue engineering. *RSC Adv.* **2020**, *10*, 40529−40542.
(45) Wang, Y.; Shi, Z.; Fang, J.; Xu, H.; Yin, J. Graphene oxide/polybenzimidazole composites fabricated by a solvent-exchange method. *Carbon* **2011**, *49*, 1199−1207.
(46) Serrano, M. C.; Patiño, J.; García-Rama, C.; Ferrer, M. L.; Fierro, J. L. G.; Tamayo, A.; Collazos-Castro, J. E.; Del Monte, F.; Gutiérrez, M. C. 3D free-standing porous scaffolds made of graphene oxide as substrates for neural cell growth. *J. Mater. Chem. B* **2014**, *2*, 5698−5706.
(47) Schacht, K.; Vogt, J.; Scheibel, T. Foams made of engineered recombinant spider silk proteins as 3D scaffolds for cell growth. *ACS Biomater. Sci. Eng.* **2016**, *2*, 517−525.
(48) Huang, J. P.; Mojib, N.; Goli, R. R.; Watkins, S.; Waites, K. B.; Ravindra, R.; Andersen, D. T.; Bej, A. K. Antimicrobial activity of PVP from an Antarctic bacterium, Janthinobacterium sp. Ant5-2, on multi-drug and methicillin resistant Staphylococcus aureus. *Nat. Prod. Bioprospect.* **2012**, *2*, 104−110.
(49) Tenover, F. C.; Arbeit, R. D.; Goering, R. V.; Mickelsen, P. A.; Murray, B. E.; Persing, D. H.; Swaminathan, B. Interpreting chromosomal DNA restriction patterns produced by pulsed-field gel electrophoresis: criteria for bacterial strain typing. *J. Clin. Microbiol.* **1995**, *33*, 2233.
(50) Zou, X.; Zhang, L.; Wang, Z.; Luo, Y. Mechanisms of the antimicrobial activities of graphene materials. *J. Am. Chem. Soc.* **2016**, *138*, 2064−2077.
(51) Guo, W.; Zhang, Y.; Feng, P.; Gao, C.; Yang, Y.; Yang, W.; Peng, S.; Shuai, C. Montmorillonite with unique interlayer space imparted polymer scaffolds with sustained release of Ag+. *Ceram. Int.* **2019**, *45*, 11517−11526.
(52) Su, H.-L.; Chou, C.-C.; Hung, D.-J.; Lin, S.-H.; Pao, I.-C.; Lin, J.-H.; Huang, F.-L.; Dong, R.-X.; Lin, J.-J. The disruption of bacterial membrane integrity through ROS generation induced by nanohybrids of silver and clay. *Biomaterials* **2009**, *30*, 5979−5987.
(53) Ruiz, O. N.; Fernando, K. A. S.; Wang, B.; Brown, N. A.; Luo, P. G.; McNamara, N. D.; Vangsness, M.; Sun, Y.-P.; Bunker, C. E. Graphene oxide: a nonspecific enhancer of cellular growth. *ACS Nano* **2011**, *5*, 8100−8107.
(54) Shen, H.; Zhang, L.; Liu, M.; Zhang, Z. Biomedical applications of graphene. *Theranostics* **2012**, *2*, 283.
(55) Yang, W.; Zhong, Y.; He, C.; Peng, S.; Yang, Y.; Qi, F.; Feng, P.; Shuai, C. Electrostatic self-assembly of pFe3O4 nanoparticles on graphene oxide: A co-dispersed nanosystem reinforces PLLA scaffolds. *J. Adv. Res.* **2020**, *24*, 191−203.
(56) Shuai, C.; Liu, G.; Yang, Y.; Qi, F.; Peng, S.; Yang, W.; He, C.; Wang, G.; Qian, G. A strawberry-like Ag-decorated barium titanate enhances piezoelectric and antibacterial activities of polymer scaffold. *Nano Energy* **2020**, *74*, 104825.
(57) Shuai, C.; Yuan, X.; Yang, W.; Peng, S.; He, C.; Feng, P.; Qi, F.; Wang, G. Cellulose nanocrystals as biobased nucleation agents in poly-l-lactide scaffold: Crystallization behavior and mechanical properties. *Polym. Test.* **2020**, *85*, 106458.

https://dx.doi.org/10.1021/acsomega.0c05596
ACS Omega 2021, 6, 4335−4346